(1H, s, aromatic), 7.21 (1H, d, J = 8.2 Hz, aromatic), 6.90 (1H, d, J = 8.2 Hz), 7.41−6.90 (4H, m, aromatic), 4.58 (1H, dd, $J_{1',2'}$ = 7.5 Hz, H-1′), 4.09−4.08 (2H, m, H-2, H-3′), 3.96−3.58 (18H, m, H-3, H-4, H-5, H-6a, H-6b, H-2′, H-4′, H-5′, H-6a′, H-6b′, H-4″, H-5″, H-6″, H-7″, H-8″, H-9a″, H-9b″, -SSCH$_2$CH$_2$CH=), 3.52−3.49 (1H, m, H-1a), 3.37−3.26 (2H, m, H-1b, -SSCH$_2$CH$_2$CH=), 3.23 (1H, ddd, J = 11.3 Hz, 6.8 Hz, 6.8 Hz, -SSCH$_2$CH$_2$CH=), 2.78−2.76 (1H, m, H-3a″), 2.59−2.52 (1H, m, -NHCOCH$_2$CH$_2$-), 2.47 (2H, t, J = 6.8 Hz, NHCOCH$_2$CH$_2$), 2.06 (3H, s, −COCH$_3$), 2.05−2.01 (1H, m, -SSCH$_2$CH$_2$CH=), 1.83−1.71 (5H, m, H-3b″, -NHCOCH$_2$CH$_2$-, -NHCOCH$_2$CH$_2$CH$_2$CH$_2$-), 1.55−1.53 (2H, m, -NHCOCH$_2$CH$_2$CH$_2$-); ESI-MS (positive mode); Found: m/z 958.2894 [(M+2Na)$^+$], Calcd. for $C_{37}H_{58}N_3O_{19}S_2Na_2$: 958.2896.

***N*-[3-[(5-Acetamido-3,5-dideoxy-D-*glycero*-α-D-galacto-2-nonulopyranosidonic acid)-(2−6)-(α-D-galactopyranosyl)-(1−4)-(1-deoxy-D-glucitol-1-yl)amino]phenyl]-DL-α-lipoamide (SAα2−6Galβ1−4Glc-mono, 6).** ^{1}H NMR (600 MHz, D$_2$O) δ 7.28 (1H, t, J = 7.5 Hz, aromatic), 7.25−7.23 (2H, m, aromatic), 6.71 (1H, d, J = 6.8 Hz, aromatic), 4.47 (1H, d, $J_{1',2'}$ = 8.2 Hz, H-1′), 4.04 (1H, m, H-2), 3.93−3.52 (19H, m, H-3, H-4, H-5, H-6a, H-6b, H-2′, H-3′, H-4′, H-5′, H-6a′, H-6b′, H-4″, H-5″, H-6″, H-7″, H-8″, H-9a″, H-9b″ -SSCH$_2$CH$_2$CH=), 3.43 (1H, dd, $J_{1a,1b}$ = 8.8 Hz, $J_{1a,2}$ = 4.1 Hz, H-1a), 3.31−3.29 (2H, m, H-1b, -SSCH$_2$CH$_2$CH=), 3.24 (1H, ddd, J = 10.7 Hz, 6.8 Hz, 6.1 Hz, -SSCH$_2$CH$_2$CH=), 2.75−2.72 (1H, m, H-3a″), 2.55 (1H, dddd, J = 12.3 Hz, 6.1 Hz, 6.1 Hz, 6.1 Hz, -SSCH$_2$CH$_2$CH=), 2.45 (2H, t, J = 6.8 Hz, -NHCOCH$_2$-), 2.06 (3H, s, −COCH$_3$), 2.04−2.02 (1H, m, -NHCOCH$_2$CH$_2$-), 1.82−1.76 (1H, m, -NHCOCH$_2$CH$_2$-), 1.86−1.69 (4H, m, H-3b″, -NHCOCH$_2$CH$_2$-, -NHCOCH$_2$CH$_2$CH$_2$-), 1.55−1.53 (2H, m, -NHCOCH$_2$CH$_2$CH$_2$-); HRMS (positive mode); Found: m/z 958.2892 [(M+2Na)$^+$], Calcd. for $C_{37}H_{58}N_3O_{19}S_2Na_2$: 958.2896.

Preparation of ZAIS/ZnS NPs. Hydrophobic ZAIS/ZnS core/shell NPs were prepared according to the method reported by Torimoto et al.[50,51] The ZAIS core were prepared by thermal decomposition of a metal ion-diethyldithiocarbamate complex of $(AgIn)_xZn_{2(1-x)}(S_2CN(C_2H_5)_2)_4$. Briefly, the complex powder was prepared by mixing 50 mL of a sodium diethyldithiocarbamate aqueous solution (50 mM) with 50 mL of an aqueous solution containing silver nitrate, indium nitrate, and zinc nitrate at a molar ratio of x:x:2(1 − x) (total concentration of metal ions: 25 mM) followed by washing with methanol several times and drying under vacuum. The complex powder (50.0 mg) was placed in a two-necked flask and heat-treated at 180 °C for 30 min in Ar atmosphere. Then, oleylamine (3 mL) was added to the obtained brown powder, followed by further heat treatment under vigorous stirring at 180 °C for 5 min in Ar atmosphere. The resulting suspension was subjected to centrifugation (4000 × g, 5 min) to remove large particles. ZAIS NPs were precipitated by the addition of methanol. Oleylamine (2 mL) was then added to the obtained precipitates. After the appropriate amounts of zinc acetate and thioacetamide at a molar ratio of 1:1 (x = 0.9: 56.3 μmol; x = 0.6: 46.1 μmol; x = 0.4: 34.8 μmol) were added, the mixture was heated at 180 °C for 30 min in Ar atmosphere to cover with the ZnS shell. The ZAIS/ZnS core/shell NPs were precipitated by the addition of methanol. The wet precipitates were dissolved in chloroform (12 mL) to give a solution of hydrophobic ZAIS/ZnS NPs.

Next, hydrophobic NPs were converted to hydrophilic NPs. To a mixture of 3-MPA solution in ethanol (200 mM, 1 mL) and KOH solution in ethanol (300 mM, 1 mL) the NPs chloroform solution (2 mL) was added at 0 °C. The mixture was then stirred at the same temperature for 3 h in the dark. The resulting precipitates were collected by centrifugal separation (4000 × g, 5 min). The precipitates were dissolved in water (2.0 mg/mL). The concentration of NPs was estimated from the absorbance at 360 nm. The obtained hydrophilic 3-MPA-capped ZAIS/ZnS NPs were treated with a solution of zinc acetate, thioacetamide, and TGA, sequentially. Zinc acetate, thioacetamide, and TGA were dissolved in water (2 mL) at a molar ratio of 1:1:1 (x = 0.9: 56.3 μmol; x = 0.6: 46.1 μmol; x = 0.4: 34.8 μmol). The pH of the mixture was adjusted to 9 with NaOH (1.0 M). The hydrophilic ZAIS/ZnS NPs solution (2 mL) was added to the mixture. The reaction mixture was stirred and heated at 80 °C for 5 h under open-air conditions. After cooling, the resulting solution was diluted with water and its concentration adjusted to 0.5 mg/mL.

Immobilization of Sugar Chain onto ZAIS/ZnS NPs. The solution of ZAIS/ZnS NPs (0.5 mg/mL, 200 μL) was concentrated by centrifugal filtration (12 000 × g, 5 min) using an Amicon Ultra 10K (Millipore, Billerica, MA, USA). The NPs were washed with water (100 μL × 2) and resuspended in water (100 μL). In another microtube, sugar chain−ligand conjugates (50 mM, 50 μL) and $NaBH_4$ aq. solution (500 mM, 50 μL,) were mixed at room temperature and the mixture was left for 10 min. The obtained solutions (each 100 μL) were then mixed and heated for 2 h in the dark at 50 °C. Excess unreacted ligand conjugates were removed by centrifugal filtration (14 000 × g, 5 min) using an Amicon Ultra 10K, and the residue was washed with water 3 times; then, PBS was added to prepare the SFNP solution.

Analysis of the Interaction between Proteins and Sugar Chains on SFNPs. The proteins, Con A, RCA120, or BSA, dissolved in PBS, were diluted sequentially. Fifty microliters of the resulting protein solution (20 μM) was placed in each well of a 96-well plate. Fifty microliters of the colloidal solution (0.5 mg/mL) was then added to the wells containing the 20 μM protein solution. After gentle agitation for 1 h, the fluorescent spectrum of the supernatant from each well was measured.

Uptake of SFNPs into Cells. THP-1 cells were placed in a cell culture flask (BD Falcon, Franklin Lakes, NJ, USA) and cultivated at 37 °C under 5% CO_2 in RPMI1640 medium containing 10% FBS and 1% PS. J774.A1 cells and HepG2 cells were placed in a cell culture flask and cultivated at 37 °C under 5% CO_2 in DMEM containing 10% FBS and 1% PS, respectively. HepG2 cells were subcultured when monolayers were 70% confluent by treatment with 0.05% trypsin containing 2 mM EDTA and then collected. For flow cytometry analysis using THP-1 and J774.A1, 5 × 10^5 cells (1 mL) were placed in microtubes and incubated in 150 μL of fresh medium (FBS- and PS-free) containing SFNPs (concentration: 100 μg/mL). After 3 h incubation at 37 or 4 °C, the medium was removed. The cells were washed with PBS (1 mL) 3 times and subjected to flow cytometry analysis. In the case of HepG2, 5 × 10^5 cells were placed in 12-well plate and incubated at 37 °C. After 48 h incubation, the medium was removed and 350 μL of fresh medium (FBS- and PS-free) containing SFNPs (concentration: 100 μg/mL) were added. After incubation for an additional 3 h at 37 or 4 °C, the medium was removed. The cells were washed with PBS (1 mL) 3 times, collected by a cell scraper (Iwaki,

Tokyo, Japan), and subjected to flow cytometry analysis. Data were accumulated using a FACS cytometer (Cytomics FC500 Cytometer). The excitation wavelength was 488 nm. Cells were gated for living cells. Fluorescence channel FL-4 was used to detect SFNP uptake by the cells. For microscopic imaging, 5×10^4 HepG2 cells were seeded in 8-well glass chamber slides. After 48 h incubation at 37 °C, the medium was removed and 100 μL of fresh medium (FBS- and PS-free) containing SFNPs (100 μg/mL) was added. After 3 h incubation at 37 °C, the cells were washed with PBS 3 times and a coverslip was placed on top of the cells. The slides were immediately observed using confocal laser scanning microscopy.

Cytotoxicity Assay of SFNPs. The cytotoxicity of SFNPs was evaluated by the MTT assay[52] and trypan blue assay with ZAIS/ZnS SFNPs and CdTe/CdS SFNPs. For the MTT assay, 1×10^5 HepG2 cells (1 mL) were placed in a 24-well plate and cultivated at 37 °C under 5% CO_2 for 24 h. The cells were then placed in fresh medium (200 μL) containing various concentrations of SFNPs (5, 25, 50, 100 μg/mL). After 24 h incubation, the cells were washed with PBS (200 μL × 3). One hundred microliters of MTT solution (5 mg/mL) were added to each well and incubated for an additional 4 h at 37 °C. The medium was removed and 1 mL of DMSO was added to each well to dissolve the MTT formazan product. After agitating for 1 h, the supernatant was recovered and the amount of MTT formazan was determined by measuring the absorbance at 540 nm using Immuno Mini NJ-2300.

For the trypan blue assay, 1×10^6 J774.A1 cells were placed in a microtube and incubated in fresh medium (200 μL) containing various concentrations of SFNPs (5, 25, 50, 100, 250 μg/mL). After 24 h incubation, 10 μL of cell suspension were transferred to a 200 μL microtube and incubated for 3 min at room temperature with an equal volume of 0.5% (w/v) trypan blue staining solution. The percentage of cell viability was determined by microscopic observation using an Olympus CKX-31 microscope with a dual-chamber hemocytometer.

For the observation of cellular morphology, 1×10^5 HepG2 cells (200 μL) were placed in 8-well glass chamber slides and cultivated for 48 h at 37 °C. The cells were placed in fresh medium (200 μL) containing various concentrations of SFNPs (5, 50 μg/mL). After 24 h incubation at 37 °C, the cells were washed with PBS (200 μL × 3), treated with a 4% formaldehyde aqueous solution for 15 min at 4 °C, and washed with PBS (200 μL × 3) again. Microscopic images were obtained using Eclipse 90i.

■ RESULTS AND DISCUSSION

Preparation of SFNPs Containing ZAIS/ZnS. Several methods for the preparation of cadmium-free fluorescent nanoparticles, such as ZnS,[53] $CuInS_2$,[54−56] ZAIS,[50,51] and InP,[57,58] have been reported. In particular, ZAIS/ZnS core/shell NPs reported by Torimoto and co-workers showed attractive optical properties and high quantum yields (up to 80%). In addition, the emission color is tunable from green to red depending on their chemical composition, and no highly toxic element was contained in their components.

The chemical formula of ZAIS is $Zn_{2(1-x)}(AgIn)_xS_2$. The photoluminescence property of ZAIS is controllable by changing the x value. In this study, we prepared ZAIS NPs with $x = 0.9$, which gives an emission peak at around 650 nm (excitation wavelength: 360 nm). The synthesis of ZAIS/ZnS core−shell NPs was carried out according to the method reported by Torimoto and co-workers, in which oleylamine was temporally coated on the NP surface.[50,51] The hydrophobic oleylamine-coated ZAIS/ZnS NPs were then converted to hydrophilic NPs by treatment with 3-MPA in EtOH, followed by sequential treatment with zinc acetate, thioacetamide, and thioglutaric acid (TGA) in water at 80 °C, affording TGA-capped ZAIS/ZnS NPs. Immobilization of sugar chains onto TGA-capped ZAIS/ZnS NPs was performed by a simple ligand-exchange reaction using our original sugar chain−ligand conjugates under reductive conditions with $NaBH_4$ (Figure 1).[49] The optimum concentration of sugar chain−ligand

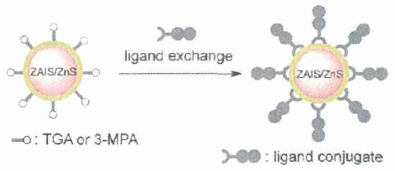

Figure 1. Preparation of SFNPs.

conjugate was examined with Glcα1−4Glc-mono ligand conjugates (**1**), which exhibited a plateau at 10−12.5 mM of the ligand conjugate (Figure 2A). The number of sugar-chain molecules per particle was estimated to be about 320 by analysis using the anthrone-sulfuric acid method,[59] which was higher than the theoretical value[60] (the number of thioctic acid as a bidentate ligand: 130 per particle; particle diameter: 4.0 nm). It is strongly suggested that most of the ligand conjugates monovalently bind to the NP surface by the treatment of excess amounts of ligand conjugates. Immobilization of the sugar moiety was qualitatively confirmed by matrix-assisted laser desorption ionization time-of-flight mass spectrometry (MALDI-TOF MS) analysis as shown in Figure 2B. A corresponding mass peak (m/z) of the used ligand conjugate was observed. The size of the obtained SFNPs was determined by transmission electron microscopy (TEM) and dynamic light scattering (DLS) analysis (Figure 2C and D). Other ligand conjugates (Galβ1−4Glc-mono [**2**], GlcNAcα1−6Glc-mono [**3**], Manα1−6Glc-mono [**4**], SAα2−3Galβ1−4Glc-mono [**5**], and SAα2−6Galβ1−4Glc-mono [**6**]) (Figure 3) were used for similarly immobilizing sugar chains onto ZAIS/ZnS NPs. All these SFNPs exhibited significant stability and high dispersibility in water or phosphate-buffered saline (PBS). Lyophilized SFNPs could be stored for at least several months in a cold chamber under dark conditions (data not shown).

Binding Experiments of SFNPs with Lectins. It is known that the interaction between sugar-chain immobilized nanoparticles and proteins possessing multiple sugar-binding sites yields aggregates and can be detected visually and spectroscopically.[19,49,61] The binding analysis of SFNPs containing ZAIS/ZnS NPs with proteins was shown in Figure 4. The proteins used were Con A (α-glucose- and α-mannose-specific), RCA120 (β-galactose-specific), and BSA (no specific binding to sugar chain). In the case of SFNPs immobilized with αGlc (αGlc-SFNP), aggregates were obtained only in the case of Con A, but not with RCA120 or BSA. When SFNPs immobilized with αGlcNAc (αGlcNAc-SFNP) were used, aggregates occurred similarly to the case of αGlc-SFNP. This result is reasonable in that the functional group at the 2-position on α-gluco- or α-mannopyranose ring does not affect the recognition of Con A. In the case of SFNPs immobilized with βGal (βGal-SFNP), aggregates were obtained in the case of RCA120, but not with Con A or BSA. On the other hand,

dx.doi.org/10.1021/bc400425w | Bioconjugate Chem. 2014, 25, 286−295

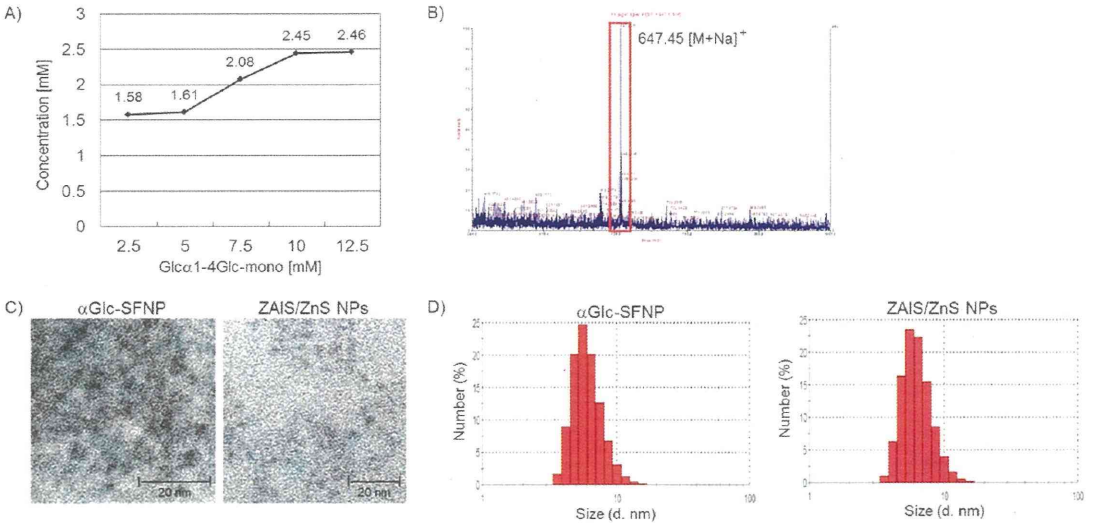

Figure 2. (A) Ligand exchange reaction under various concentrations of **1**. (B) MS analysis of SFNPs prepared with **1**. The detected peak was 647.45 $[M+Na]^+$. (C) TEM imaging of SFNPs (x = 0.9) prepared with **1** and ZAIS/ZnS (x = 0.9) NPs stabilized with TGA. The average diameter was about 4.0 nm. Scale bar: 20 nm. (D) Histogram of DLS data of SFNPs prepared using Glcα1−4Glc-mono and NPs stabilized with TGA. Average hydrodynamic diameter was about 6.2 nm.

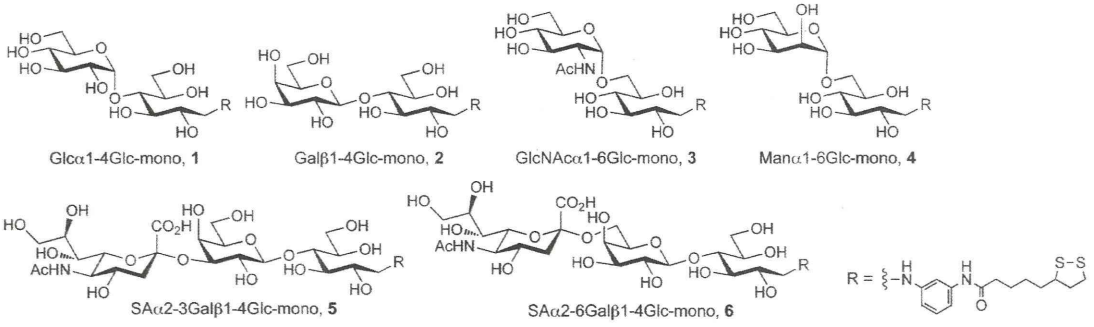

Figure 3. Sugar-chain−ligand conjugates used in this study.

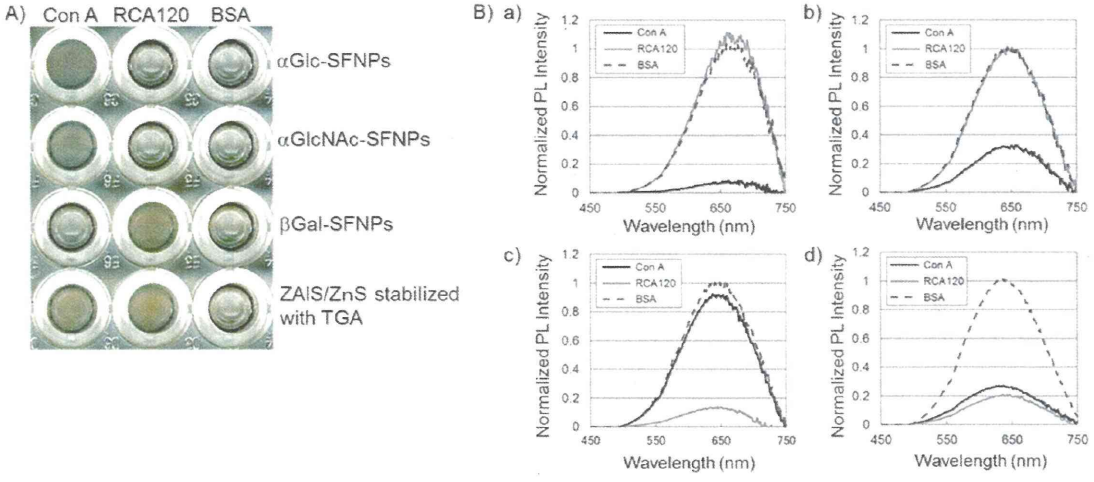

Figure 4. Interaction analysis between SFNPs and proteins. (A) Visual image. Each SFNPs was mixed with protein. (B) The fluorescent spectrum of supernatant monitored by excitation wavelength at 400 nm. (a) αGlc-SFNP, (b) αGlcNAc-SFNP, (c) βGal-SFNP, (d) ZAIS/ZnS stabilized with TGA.

dx.doi.org/10.1021/bc400425w | *Bioconjugate Chem.* 2014, 25, 286−295

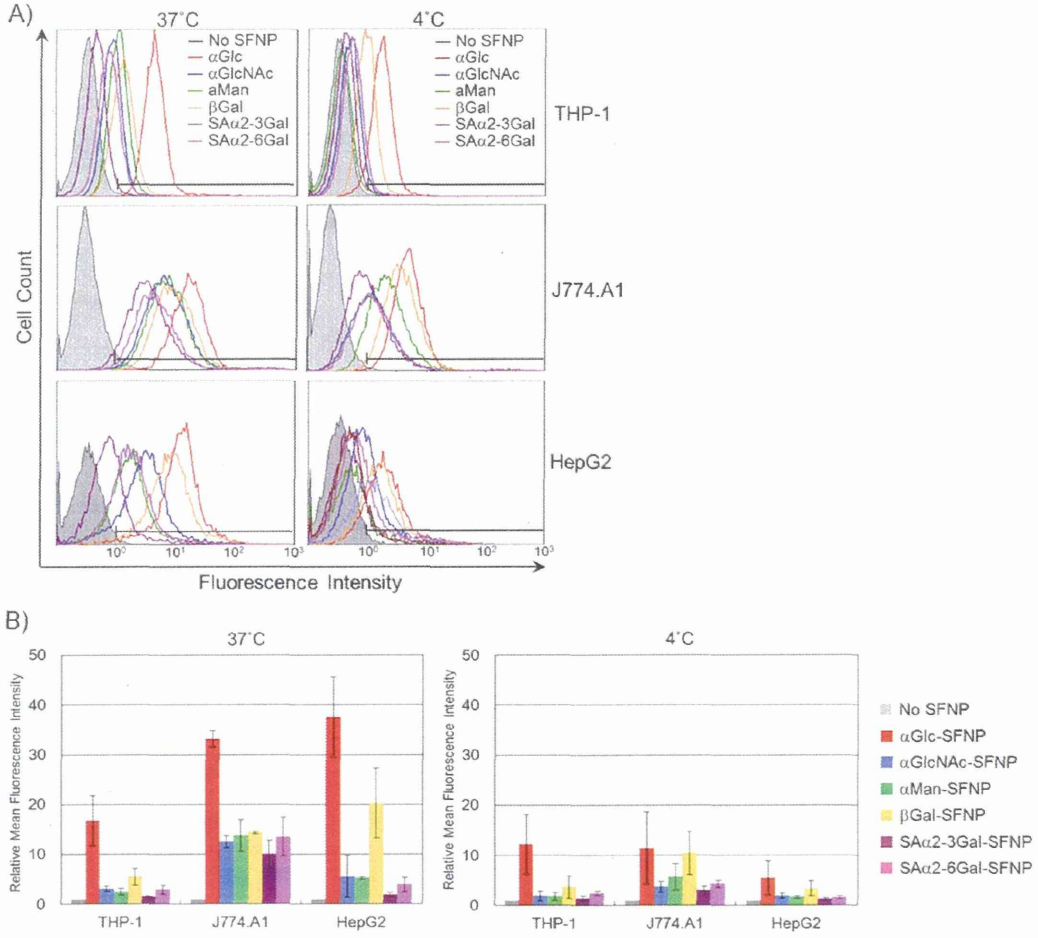

Figure 5. Flow cytometry analysis. The histogram of each cell incubated at 37 °C (left) or 4 °C (right) (A) and relative mean fluorescence intensity (MFI, B). The excitation wavelength in the FACS experiment was 488 nm. Cells were gated on living cells and FL-4 was used as a fluorescence channel to detect each cell labeled with SFNPs.

when TGA capped ZAIS/ZnS NPs were mixed with protein, aggregates were formed in both case of Con A and RCA120, indicating nonspecific binding. In fluorescent spectra, a decrease in the fluorescent intensity of the supernatant was observed (Figure 4B) due to the specific binding of protein to SGNPs. Thus, SFNPs containing ZAIS/ZnS NPs are applicable for both visual and fluorescent detection of sugar chain–protein interaction, the same as SFNPs containing CdTe/CdS.

Cellular Uptake of SFNPs. Following the successful binding experiments of SFNPs with proteins, the SFNPs were applied to cellular labeling and imaging. Various sugar chain-binding receptor proteins are expressed on the cell surface. The evaluation of the sugar chain-binding properties of the cell provides functional information on the cell and classifies the cell type. In the binding experiments, 3 kinds of cell lines, a human acute monocytic leukemia cell line (THP-1), a murine macrophage cell line (J774.A1), and a human hepatic carcinoma cell line (HepG2), and 6 kinds of SFNPs, αGlc-SFNP, βGal-SFNP, αGlcNAc-SFNP, αMan-FNP (FNPs with immobilized **4**), SAα2−3Gal-SFNP (FNPs with immobilized **5**), and SAα2−6Gal-SFNP (FNPs immobilizing **6**) were used. The results of flow cytometry analysis are shown in Figure 5. Mean fluorescence intensity (MFI) was calculated from fluorescence intensity per cell. The relative MFI value was calculated based on the value when cells were incubated without SFNPs. After 3 h of incubation, different cellular uptake of SFNPs was observed on the basis of the sugar-chain type. αGlc-SFNPs were found to bind to all 3 types of cell lines. This binding may occur by the interaction with the glucose transporter, since cells express the protein on the surface to take up glucose as an energy source.[62] In the binding analysis with THP-1 cells, the SFNPs, except those with αGlc, showed low affinity compared to that seen with other cells. THP-1 cells are known to be immature hematopoietic cells and may not express enough amounts of sugar-binding receptors. On the other hand, J774.A1 cells, mature macrophage cells, showed high binding affinities for all the SFNPs. Mature macrophage cells are known to express various sugar-chain binding receptors such as mannose-binding protein (MBP),[63] galectin (galactose-binding protein),[64,65] and sialoadhesin (sialic acid-binding protein).[66,67] The two former receptors are involved in the phagocytotic clearance of microorganisms. The latter is related to their migration and infiltration. In the case of HepG2 cells, βGal-SFNP predominantly bound to the cells. Hepatic cells normally express asialoglycoprotein receptor,[68−71] which recognizes the terminal galactose moiety to remove asialogly-

dx.doi.org/10.1021/bc400425w | Bioconjugate Chem. 2014, 25, 286−295

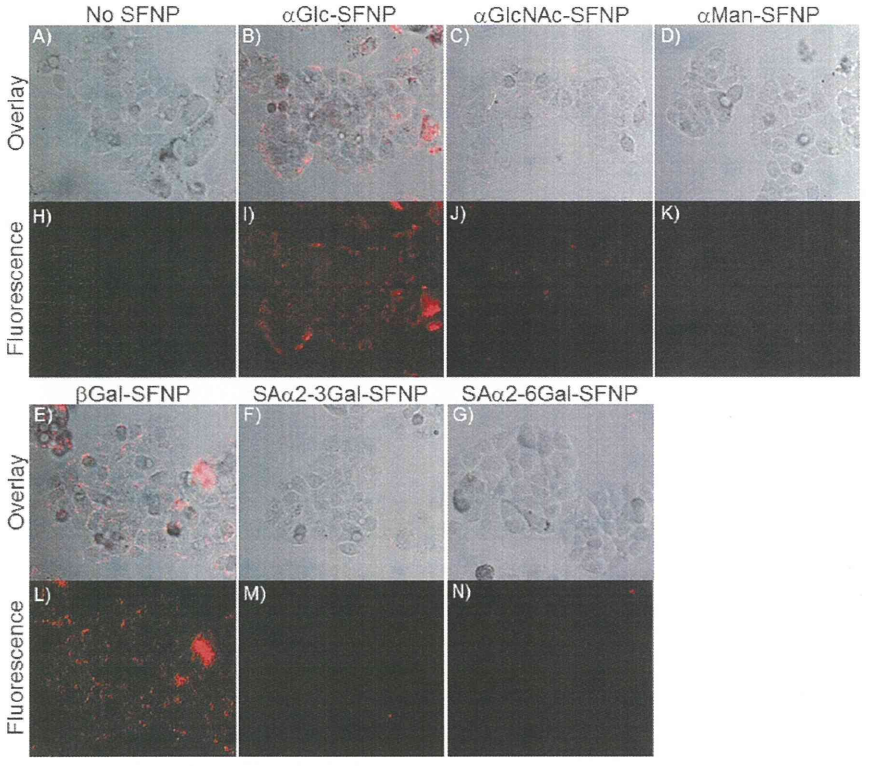

Figure 6. Confocal laser scanning microscopic imaging of HepG2 cells. Overlay images (top panel, A–G) and fluorescence images (lower panel H–N). HepG2 cells were incubated without SFNPs (A and H) and with αGlc-SFNPs (B and I), αGlcNAc-SFNPs (C and J), βGal-SFNPs (D and K), SAα2–3Gal-SFNPs (F and M), or SAα2–6Gal-SFNPs (G and N).

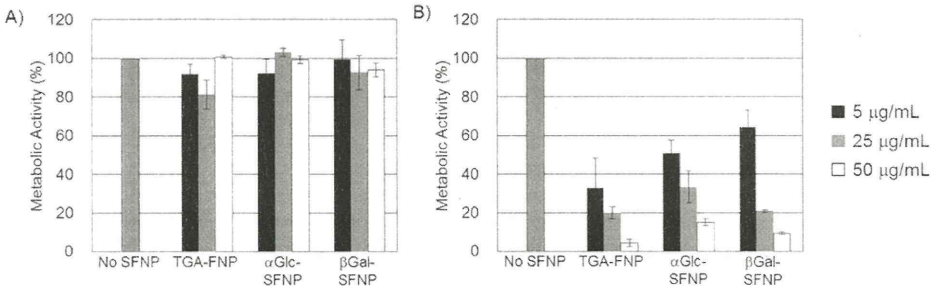

Figure 7. MTT assay for SFNPs. HepG2 cells were incubated with ZAIS/ZnS NPs (A) or CdTe/CdS QDs (B). The nanoparticle concentration was in the range of 5 μg/mL to 50 μg/mL (left to right).

coproteins. On the other hand, the binding intensity of the cells incubated at 4 °C was significantly decreased compared with cells incubated at 37 °C. These results indicate that SFNPs not only bound to the cell surface but were also internalized into the cells by endocytosis. Confocal laser scanning imaging for HepG2 cells yielded results similar to that of fluorescent-activated cell sorting (FACS) analysis, which showed that αGlc-SFNP and βGal-SFNP were predominantly taken up while αGlcNAc-SFNP, SAα2–3Gal-SFNP, and SAα2–6Gal-SFNP were only slightly taken up (Figure 6). Thus, our prepared SFNPs are useful for the analysis and imaging of cells on the basis of sugar chain–protein interactions, and can be applicable to cell profiling.

Cytotoxicity Assay of SFNPs. The cytotoxic activity of SFNPs was evaluated by the MTT assay and morphological analysis. In this assay, HepG2 cells were used. CdTe/CdS QDs were used for comparing cytotoxicity. In addition, to investigate the effect of capping agents, three kinds of capping agents, **1**, **2**, and TGA, were used. TGA-capped CdTe/CdS QDss and CdTe/CdS SFNPs were prepared according to our previous method.[49] The results of the MTT assay after 24 h incubation are shown in Figure 7. Interestingly, the metabolic activity of cells treated with ZAIS/ZnS NPs was similar to that of untreated cells (Figure 7A). The morphology of cells treated with ZAIS/ZnS SFNPs was also the same as that of untreated cells (Figure 8D and E). These data indicate that ZAIS/ZnS NPs were nontoxic in the concentration range of 5–50 μg/mL. On the other hand, treatment with CdTe/CdS SFNPs dramatically decreased metabolic activity (Figure 7B), although capping of the QDs with sugar-chain–ligand conjugates such as

dx.doi.org/10.1021/bc400425w | Bioconjugate Chem. 2014, 25, 286–295

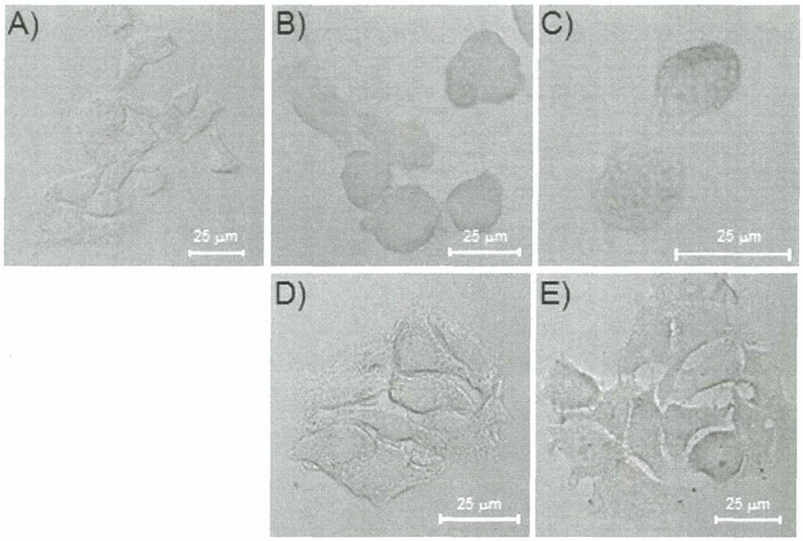

Figure 8. Microscopic images of HepG2 incubated for 24 h without SFNPs (A), with 5 μg/mL of CdTe/CdS βGal-SFNPs (B), with 50 μg/mL of CdTe/CdS βGal-SFNPs (C), with 5 μg/mL of ZAIS/ZnS βGal-SFNPs (D), and with 50 μg/mL of ZAIS/ZnS βGal-SFNPs (E).

1 and **2** slightly suppressed the cytotoxicity of CdTe/CdS QDs. In the morphological study, cells treated with CdTe/CdS SFNPs showed shrinkage, exhibiting cytotoxicity that may be caused by Cd^{2+} ions.[38] Thus, our newly developed ZAIS/ZnS SFNPs appear to be highly promising tools for in vitro and in vivo cell analysis because of their negligible cytotoxicity.

In this study, we successfully synthesized cadmium-free SFNPs containing low-toxicity ZAIS/ZnS NPs as the core and demonstrated their usefulness in the visual and fluorescent detection of sugar-chain–protein interactions, as well as in cellular imaging. The sugar-chain–ligand conjugate was easily immobilized onto the ZAIS NP surface by a simple ligand exchange reaction and could be applied to various sugar-chain–ligand conjugates. The binding interaction of the SFNPs with lectin was detected visually and spectroscopically. In flow cytometry analysis and cellular imaging, the binding properties of the SFNPs were diverse depending on the cell type, which may have great potential for profiling cells based on their sugar-chain binding properties. The results of the cytotoxicity assay showed that ZAIS/ZnS SFNPs were less toxic than CdTe/CdS SFNPs. Thus, our developed SFNPs are environmentally friendly compared with other cadmium-based semiconductor NPs and are likely to prove significantly useful for investigating various sugar-chain functions.

AUTHOR INFORMATION

Corresponding Authors

*TEL: (+81)99-285-7843, FAX: (+81)99-285-7856, E-mail: wakao@eng.kagoshima-u.ac.jp.
*TEL and FAX: (+81)99-285-8369.

Notes

The authors declare no competing financial interest.

ACKNOWLEDGMENTS

The present study was financially supported in part by grants from Japan Science and Technology Agency (Evolutionally venture program V07-05 to Y.S., CREST to Y.S., Research for Promoting Technological Seeds 16-057 to M.W., A-STEP AS242Z02646P to M.W.).

REFERENCES

(1) Varki, A. (1993) Biological roles of oligosaccharides: all of the theories are correct. *Glycobiology* 3, 97–130.
(2) Opdenakker, G., Rudd, P. M., Ponting, C. P., and Dwek, R. A. (1993) Concepts and princiles of Glycobiology. *FASEB J.* 7, 1330–1337.
(3) Park, S., and Shin, I. (2002) Fabrication of carbohydrate chips for studying protein-carbohydrate interactions. *Angew. Chem., Int. Ed.* 41, 3180–3182.
(4) Wang, D., Liu, S., Trummer, B. J., Deng, C., and Wang, A. (2002) Carbohydrate microarrys for the recognition of cross-reactive molecular markers of microbes and host cells. *Nat. Biotechnol.* 20, 275–281.
(5) Fukui, S., Feizi, T., Galustian, C., Lawson, A. M., and Chai, W. (2002) Oligosaccharide microarrays for high-throughput detection and specificity assignments of carbohydrate-protein interactions. *Nat. Biotechnol.* 20, 1011–1017.
(6) Fazio, F., Bryan, M. C., Blixt, O., Paulson, J. C., and Wong, C.-H. (2002) Synthesis of sugar arrays in microtiter plate. *J. Am. Chem. Soc.* 124, 14397–14402.
(7) Mann, D. A., Kanai, M., Maly, D. J., and Kiessling, L. L. (1998) Probing low affinity and multivalent interactions with surface plasmon resonance: ligands for concanavalin A. *J. Am. Chem. Soc.* 120, 10575–10582.
(8) Horan, N., Yan, L., Isobe, H., Whitesides, G. M., and Kahne, D. (1999) Nonstatical binding of a protein to clustered carbohydrates. *Proc. Natl. Acad. Sci. U.S.A.* 96, 11782–11786.
(9) Oyelaran, O., and Gildersleeve, J. C. (2009) Glycan arrays: recent advances and future challenges. *Curr. Opin. Chem. Biol.* 13, 406–413.
(10) Hase, S., Ibuki, T., and Ikenaka, T. (1984) Reexamination of the pyridylamination used for fluorescence labeling of oligosaccharides and its application to glycoproteins. *J. Biochem.* 95, 197–203.
(11) Anumula, K. R. (2006) Advances in fluorescence derivatization methods for high-performance liquid chromatographic analysis of glycoprotein carbohydrates. *Anal. Biochem.* 350, 1–23.
(12) Reddington, M. V. (1998) New glycoconjugated cyanine dyes as fluorescent labeling reagents. *J. Chem. Soc., Perkin Trans.*, 143–147.

(13) Gege, C., Oscarson, S., and Schmidt, R. R. (2001) Synthesis of fluorescence labeled sialyl lewis(x) glycosphingolipids. *Tetrahedron Lett. 42*, 377−380.
(14) de la Fuente, J. M., Barrientos, A. G., Rojas, T. C., Rojo, J., Cañada, J., Fernández, A., and Penadés, S. (2001) Gold glyconanoparticles as water-soluble polyvalent models to study carbohydrate interactions. *Angew. Chem., Int. Ed. 40*, 2258−2261.
(15) Osaki, F., Kanamori, T., Sando, S., Sere, T., and Aoyama, Y. (2004) A quantum dot conjugated sugar ball and its cellular uptake. on the size effects of endocytosis in the subviral region. *J. Am. Chem. Soc. 126*, 6520−6521.
(16) Sun, X.-L., Cui, W., Haller, C., and Chaikof, E. L. (2004) Site-specific multivalent carbohydrate labeling of quantum dots and magnetic beads. *ChemBioChem 5*, 1593−1596.
(17) de la Fuente, J. M., and Penadés, S. (2005) Glyco-quantum dots: a new luminescent system with multivalent carbohydrate display. *Tetrahedron: Asymmetry 16*, 387−391.
(18) Robinson, A., Fang, J.-M., Chou, P.-T., Liao, K.-W., Chu, R.-M., and Lee, S.-J. (2005) Probing lectin and sperm with carbohydrate-modified quantum dots. *ChemBioChem 6*, 1899−1905.
(19) Babu, P., Sinha, S., and Surolia, A. (2007) Sugar-quantum dot conjugates for selective and sensitive detection of lectins. *Bioconjugate Chem. 18*, 146−151.
(20) Niikura, K., Nishio, T., Akita, H., Matsuo, Y., Kamitani, R., Kogure, K., Harashima, H., and Ijiro, K. (2007) Accumulation of O-GlcNAc-displaying CdTe quantum Dots in cells in the presence of ATP. *ChemBioChem 8*, 379−384.
(21) Kikkeri, R., Lepenies, B., Adibekian, A., Laurino, P., and Seeberger, P. H. (2009) In vivo imaging and in vitro liver targeting with carbohydrate capped quantum dots. *J. Am. Chem. Soc. 131*, 2110−2112.
(22) Marradi, M., Martín-Lomas, M., and Penadés, S. (2010) Glyconanoparticles: polyvalent tools to study carbohydrate-based interactions. *Adv. Carbohydr. Chem. Biochem. 64*, 211−290.
(23) Varki, A., and Marth, J. (1995) Oligosaccharides in vertebrate development. *Semin. Dev. Biol. 6*, 127−138.
(24) Gabius, H.-J., André, S., Kaltner, H., and Siebert, H.-C. (2002) The sugar code: functional lectinomics. *Biochim. Biophys. Acta 1572*, 165−177.
(25) Sharon, N., and Lis, H. (2004) History of lectins: from hemagglutinins to biological recognition molecules. *Glycobiology 14*, 53R−62R.
(26) Ilyin, S. E., Belkowski, S. M., and Plata-Salamán, C. R. (2004) Biomarker discovery and validation: technologies and integrative approaches. *TRENDS Biotechnol. 22*, 411−416.
(27) Rifai, N., Gillette, M. A., and Carr, S. A. (2006) Protein biomarker discovery and validation: the long and uncertain path to clinical utility. *Nat. Biotechnol. 24*, 971−983.
(28) Nagano, K., Yoshida, Y., and Isobe, T. (2008) Cell surface biomarkers of embryonic stem cells. *Proteomics 8*, 4025−4035.
(29) Tateno, H., Uchiyama, N., Kuno, A., Togayachi, A., Sato, T., Narimatsu, H., and Hirabayashi, J. (2007) A novel strategy for mammalian cell surface glycome profiling using lectin microarray. *Glycobiology 17*, 1138−1146.
(30) Toyoda, M., Yamazaki-Inoue, M., Itakura, Y., Kuno, A., Ogawa, T., Yamada, M., Akutsu, H., Takahashi, Y., Kanzaki, S., Narimatsu, H., Hirabayashi, J., and Umezawa, A. (2011) Lectin microarray analysis of pluripotent and multipotent stem cells. *Genes Cells 16*, 1−11.
(31) Jeong, H. H., Kim, Y. G., Jang, S. C., Yi, H., and Lee, C. S. (2012) Profiling surface glycan on live cells and tissues using quantum dot-lectin nanoconjugates. *Lab Chip 12*, 3290−3295.
(32) Nishijima, Y., Toyoda, M., Yamazaki-Inoue, M., Sugiyama, T., Miyazawa, M., Muramatsu, T., Nakamura, K., Narimatsu, H., Umezawa, A., and Mikami, M. (2012) Glycan profiling of endometrial cancers using lectin microarray. *Genes Cells 17*, 826−836.
(33) Alivisatos, A. P. (1996) Semiconductor clusters, nanocrystals, and quantum dots. *Science 271*, 933−937.
(34) Bruchez, M., Moronne, M., Gin, P., Weiss, S., and Alivistos, A. P. (1998) Semiconductor nanocrystals as fluorescent biological labels. *Science 281*, 2031−2016.
(35) Chan, W. C. W., and Nie, S. M. (1998) Quantum dot bioconjugates for ultrasensitive nonisotopic detection. *Science 281*, 2016−2018.
(36) Akerman, M. E., Chan, W. C. W., Laakkonen, P., Bhatia, S. N., and Ruslahti, E. (2002) Nanocrystal targeting in vivo. *Proc. Natl. Acad. Sci. U.S.A. 99*, 12617−12621.
(37) Walling, M. A., Novak, J. A., and Shepard, J. R. E. (2009) Quantum dots for live cell and in vivo imaging. *Int. J. Mol. Sci. 10*, 441−491.
(38) Ipe, B. I., Lehnig, M., and Niemeyer, C. M. (2005) On the generation of free radical species from quantum dots. *Small 1*, 706−709.
(39) Hardman, R. (2006) A toxicologic review of quantum dots: toxicity depends on physicochemical and environmental factors. *Env. Health Persp. 114*, 116−172.
(40) Chang, E., Thekkek, N., Yu, W. W., Colvin, V. L., and Drezek, R. (2006) Evaluation of quantum dot cytotoxicity based on intracellular uptake. *Small 2*, 1412−1417.
(41) Chang, S.-Q., Dai, Y.-D., Kang, B., Han, W., Mao, L., and Chen, D. (2009) UV-enhanced cytotoxicity of thiol-capped CdTe quantum dots in human pancreatic carcinoma cells. *Toxicol. Lett. 188*, 104−111.
(42) Rzigalinski, B. A., and Strobl, J. S. (2009) Cadmium-containing nanoparticles: perspectives on pharmacology and toxicology of quantum dots. *Toxicol. Appl. Pharmacol. 238*, 280−288.
(43) Ballou, B., Lagerholm, B. C., Ernst, L. A., Bruchez, M. P., and Waggoner, A. S. (2004) Noninvasive imaging of quantum dots in mice. *Bioconjugate Chem. 15*, 79−86.
(44) Hoshino, A., Fujioka, K., Oku, T., Suga, M., Sasaki, F. Y., Ohta, T., Yasuhara, M., Suzuki, K., and Yamamoto, K. (2004) Physicochemical properties and cellular toxicity of nanocrystal quantum dots depend on their surface modification. *Nano Lett. 4*, 2163−2169.
(45) Shiohara, A., Hoshino, A., Hanaki, K., Suzuki, K., and Yamamoto, K. (2004) On the cytotoxicity of quantum dots. *Microbiol. Immunol. 48*, 669−675.
(46) Kim, J., Park, Y., Yoon, T. H., Yoon, C. S., and Choi, K. (2010) Phototoxicity of CdSe/ZnSe quantum dots with surface coatings of 3-mercaptopropionic acid or tri-*n*-octylphosphine oxide/gum arabic in Daphnia magna under environmentally relevant UV-B light. *Aquatic Toxicol. 97*, 116−124.
(47) Suda, Y., Arano, A., Fukui, Y., Koshida, S., Wakao, M., Nishimura, T., Kusumoto, S., and Sobel, M. (2006) Immobilization and clustering of structurally defined oligosaccharides for sugar chips:an improved method for surface plasmon resonance analysis of protein−carbohydrate interactions. *Bioconjugate Chem. 17*, 1125−1135.
(48) Zhang, X., Nakamura-Tsuruta, S., Haruyama, M., Yokoyama, R., Nagatomo, M., Wakao, M., Nakajima, K., Aoyama, K., Okuno, T., Morikawa, S., Hiroi, S., Kase, T., Nose, H., Nishi, J., Okamoto, M., Baba, M., and Suda, Y. (2012) Super sensitive detection of viruses using sugar-chain immobilized gold nano-particles (SGNPs). *Polym. Prepr. 53*, 671−672.
(49) Shinchi, H., Wakao, M., Nakagawa, S., Mochizuki, E., Kuwabata, S., and Suda, Y. (2012) Stable sugar-chain immobilized fluorescent nano-particle for probing lectin and cells. *Chem.-Asian J. 7*, 2678−2682.
(50) Torimoto, T., Adachi, T., Okazaki, K., Sakuraoka, M., Shibayama, T., Ohtani, B., Kudo, A., and Kuwabata, S. (2007) Facile synthesis of ZnS-$AgInS_2$ solid solution nanoparticles for color-adjustable luminophore. *J. Am. Chem. Soc. 129*, 12388−12389.
(51) Torimoto, T., Ogawa, S., Adachi, T., Kameyama, T., Okazaki, K., Shibayama, T., Kudo, A., and Kuwabata, S. (2010) Remarkable photoluminescence enhancement of ZnS-$AgInS_2$ solid solution nanoparticles by postsynthesis treatment. *Chem. Commun. 46*, 2082−2084.

(52) Mosmann, T. (1983) Rapid colorimetric assay for cellular growth and survival: application to proliferation and cytotoxicity assays. *J. Immun. Methods. 65*, 55–63.
(53) Kuzuya, T., Tai, Y., Yamamuro, S., and Sumiyama, K. (2005) Synthesis of copper and zinc sulfide nanocrystals via thermolysis of the polymetallic thiolate cage. *Sci. Technol. Adv. Mater. 6*, 84–90.
(54) Castro, S. L., Bailey, S. G., Raffaelle, R. P., Banger, K. K., and Hepp, A. F. (2003) Nanocrystalline chalcopyrite materials ($CuInS_2$ and $CuInSe_2$) via low-temperature pyrolysis of molecurlar single-source precursors. *Chem. Mater. 15*, 3142–3147.
(55) Li, L., Daou, T. J., Texier, I., and Kim, T. T. (2009) Highly luminescent $CuInS_2$/ZnS core/shell nanocrystals: cadmium-free quantum dots for in vivo imaging. *Chem. Mater. 21*, 2422–2429.
(56) Pons, T., Pic, E., Lequeux, N., Cassette, E., Bezdetnaya, L., Guillemin, F., Marchal, F., and Dubertret, B. (2010) Cadmium-free $CuInS_2$/ZnS quantum dots for sentinel lymph node imaging with reduced toxicity. *ACS Nano 4*, 2531–2538.
(57) Matsumoto, T., Maenosono, S., and Yamaguchi, Y. (2004) Organometallic synthesis of InP quantum dots using tris-(dimethylamino)phosphine as a phosphorus source. *Chem. Lett. 33*, 1492–1493.
(58) Li, C., Ando, M., Enomoto, H., and Murase, N. (2008) Highly luminescent water-soluble InP/ZnS nanocrystals prepared via reactive phase transfer and photochemical processing. *J. Phys. Chem. C 112*, 20190–20199.
(59) Roe, J. H. (1955) The determination of sugar in blood and spinal fluid with anthrone reagent. *J. Biol. Chem. 212*, 335–343.
(60) Prasuhn, E. D., Deschamps, J. R, Susumu, K., Stewart, M. H., Boeneman, K., Blanco-Canosa, J. B., Dawson, P. E., and Medintz, I. L. (2010) Polyvalent display and packing of peptides and proteins on semiconductor quantum dots: predicted versus experimental results. *Small 6*, 555–564.
(61) Nakamura-Tsuruta, S., Kishimoto, Y., Nishimura, T., and Suda, Y. (2008) One-step purification of lectins from Banana pulp using sugar-immobilized gold nano-particles. *J. Biochem. 143*, 833–839.
(62) Wood, I. S., and Trayhurn, P. (2003) Glucose transporters (GLUT and SGLT): expanded families of sugar transport proteins. *Br. J. Nutr. 89*, 3–9.
(63) Stahl, P. D. (1992) The mannose receptor and other macrophage lectins. *Curr. Opin. Immunol. 4*, 49–52.
(64) Sato, S., and Hughes, R. C. (1994) Regulation of secretion and surface expression of Mac-2, a galactoside-binding protein of macrophages. *J. Biol. Chem. 269*, 4424–4430.
(65) Sano, H., Hsu, D. K., Apgar, J. R., Yu, L., Sharma, B. B., Kuwabara, I., Izui, S., and Liu, F.-T. (2003) Critical role of galectin-3 phagocytosis by macrophages. *J. Clin. Invest. 112*, 389–397.
(66) Crocker, P. R., Mucklow, S., Bouckson, V., McWilliam, A., Willis, A. C., Gordon, S., Milon, G., Kelm, S., and Bradfield, P. (1994) Sialoadhesin, a macrophage sialic acid binding receptor for haemopoietic cells with 17 immunoglobulin-like domains. *EMBO J. 13*, 4490–4503.
(67) Jones, C., Virji, M., and Crocker, R. (2003) Recognition of sialylated meningococcal lipopolysaccharide by siglecs expressed on myeloid cells leads to enhanced bacterial uptake. *Mol. Microbiol. 49*, 1213–1225.
(68) Baenziger, J. U., and Fiete, D. (1980) Galactose and N-acetylgalactosamaine-specific endocytosis of glycopeptides by isolated rat hepatocytes. *Cell 22*, 611–620.
(69) Ashwell, G., and Harford, J. (1982) Carbohydrate-specific receptors of the liver. *Annu. Rev. Biochem. 51*, 531–554.
(70) Braun, J. R., Willnow, T. E., Ishibashi, S., Ashwell, G., and Herz, J. (1996) Sugar chains, lipids, and other natural products. *J. Biol. Chem. 271*, 21160–21166.
(71) Raju, T. S., Briggs, J. B., Chamow, S. M., Winkler, M. E., and Jones, A. J. S. (2001) Glycoengineering of therapeutic glycoproteins: in vitro galactosylation and sialylation of glycoproteins with terminal N-acetylglucosamine and galactose residue. *Biochemistry 40*, 8868–8876.

EWS/ATF1 expression induces sarcomas from neural crest–derived cells in mice

Kazunari Yamada,[1,2] Takatoshi Ohno,[1] Hitomi Aoki,[3] Katsunori Semi,[4,5] Akira Watanabe,[4,5] Hiroshi Moritake,[6] Shunichi Shiozawa,[7] Takahiro Kunisada,[3] Yukiko Kobayashi,[8] Junya Toguchida,[4,8,9] Katsuji Shimizu,[1] Akira Hara,[2] and Yasuhiro Yamada[2,4,5]

[1]Department of Orthopedic Surgery, [2]Department of Tumor Pathology, and [3]Department of Tissue and Organ Development Regeneration and Advanced Medical Science, Gifu University Graduate School of Medicine, Gifu, Japan.
[4]Center for iPS Cell Research and Application (CiRA) and [5]Institute for Integrated Cell-Material Sciences, (WPI-iCeMS), Kyoto University, Kyoto, Japan.
[6]Division of Pediatrics, Department of Reproductive and Developmental Medicine, Faculty of Medicine, University of Miyazaki, Miyazaki, Japan.
[7]Department of Medicine, Kyushu University Beppu Hospital, Beppu, Japan. [8]Department of Tissue Regeneration, Institute for Frontier Medical Sciences, and [9]Department of Orthopaedic Surgery, Kyoto University, Kyoto, Japan.

Clear cell sarcoma (CCS) is an aggressive soft tissue malignant tumor characterized by a unique t(12;22) translocation that leads to the expression of a chimeric *EWS/ATF1* fusion gene. However, little is known about the mechanisms underlying the involvement of *EWS/ATF1* in CCS development. In addition, the cellular origins of CCS have not been determined. Here, we generated *EWS/ATF1*-inducible mice and examined the effects of *EWS/ATF1* expression in adult somatic cells. We found that forced expression of *EWS/ATF1* resulted in the development of *EWS/ATF1*-dependent sarcomas in mice. The histology of *EWS/ATF1*-induced sarcomas resembled that of CCS, and *EWS/ATF1*-induced tumor cells expressed CCS markers, including S100, SOX10, and MITF. Lineage-tracing experiments indicated that neural crest–derived cells were subject to *EWS/ATF1*-driven transformation. EWS/ATF1 directly induced Fos in an ERK-independent manner. Treatment of human and *EWS/ATF1*-induced CCS tumor cells with FOS-targeted siRNA attenuated proliferation. These findings demonstrated that FOS mediates the growth of *EWS/ATF1*-associated sarcomas and suggest that FOS is a potential therapeutic target in human CCS.

Introduction

Clear cell sarcoma (CCS) is an aggressive malignancy of adolescents and young adults that was first described by Enzinger (1). It typically arises in the deep soft tissues of the lower extremities closed to tendon, fascia, and aponeurosis (2). Chemotherapy and radiotherapy are not of any benefit (3–5), and a high rate of local and distant recurrence results in poor survival rates (3, 6, 7). CCSs harbor the potential for melanocytic differentiation and melanin synthesis (8). Gene expression profiles support the classification of CCS as a distinct genomic subtype of melanomas (9). These melanocytic features often make the distinction from malignant melanoma (MM) difficult. However, in contrast to MM, CCS is characterized by a chromosomal translocation, t(12;22)(q13;q12), that leads to the fusion of activating transcription factor 1 (*ATF1*) gene localized to 12q13 to Ewing's sarcoma oncogene (*EWS*) gene at 22q12 in up to 90% of cases, resulting in expression of the *EWS/ATF1* fusion gene (10–12). Given that CCS and MM have such similar characteristics, it has been proposed that CCSs may arise from a neural crest progenitor. However, the exact origin of CCS still remains to be determined.

The biological role of the EWS/ATF1 fusion protein is still unclear. EWS contains a transcriptional activation domain in the N-terminal region (13–15) and several conserved RNA binding motifs in the C-terminal region (16). Binding of the N-terminal region of EWS to the RNA polymerase II subunit hsRPB7 has been proposed to be important for transactivation of the target genes (17). In contrast, ATF1 is a member of the CREB transcription factor family, whose activity is regulated through phosphorylation of its kinase inducible domain (KID) by protein kinase A (18). ATF1 mediates the activation of cAMP-responsive genes through binding to a conserved cAMP-responsive element (CRE) as a dimmer (19, 20). However, the N-terminal activation domain of EWS replaces the KID in the EWS/ATF1 fusion protein, rendering it unable to support a typical inductive signal (21). Therefore, EWS/ATF1 can act as constitutive transcriptional activator in a cAMP-independent fashion with normal CRE DNA binding activity (14, 22, 23).

Previous studies have revealed some target genes of EWS/ATF1, but their true function in tumorigenesis is still not well understood (24). Expression of *MITF* is constitutively activated by *EWS/ATF1* in CCS in vitro (25). Consistent with this finding, several studies have identified the expression of MITF protein or mRNA in CCS (26–28). MITF is a master regulator of melanocyte development and plays a role in melanoma development (29, 30). Importantly, activation of MITF by EWS/ATF1 is required for CCS proliferation as well as for melanocytic differentiation of CCS in vitro (25).

Although previous studies have demonstrated that EWS/ATF1 is associated with oncogenic potential in CCS, the effect of in vivo expression of *EWS/ATF1* on sarcoma formation is still not known. In the present study, we established *EWS/ATF1* transgenic mice using a doxycycline-dependent expression system in order to investigate the role of *EWS/ATF1* on CCS development in vivo. Our results showed that forced expression of *EWS/ATF1* induced CCS-like sarcoma in the transgenic mice. This mouse model was used to identify the origin of *EWS/ATF1*-induced sarcomas as well as the direct target of EWS/ATF1 in these sarcomas.

Results

Inducible expression of EWS/ATF1 in mice. We first generated doxycycline-inducible *EWS/ATF1* ES cells, in which the human *EWS/ATF1* type 2 fusion gene (26, 31) can be induced under the control of

Conflict of interest: The authors have declared that no conflict of interest exists.
Citation for this article: *J Clin Invest.* doi:10.1172/JCI63572.

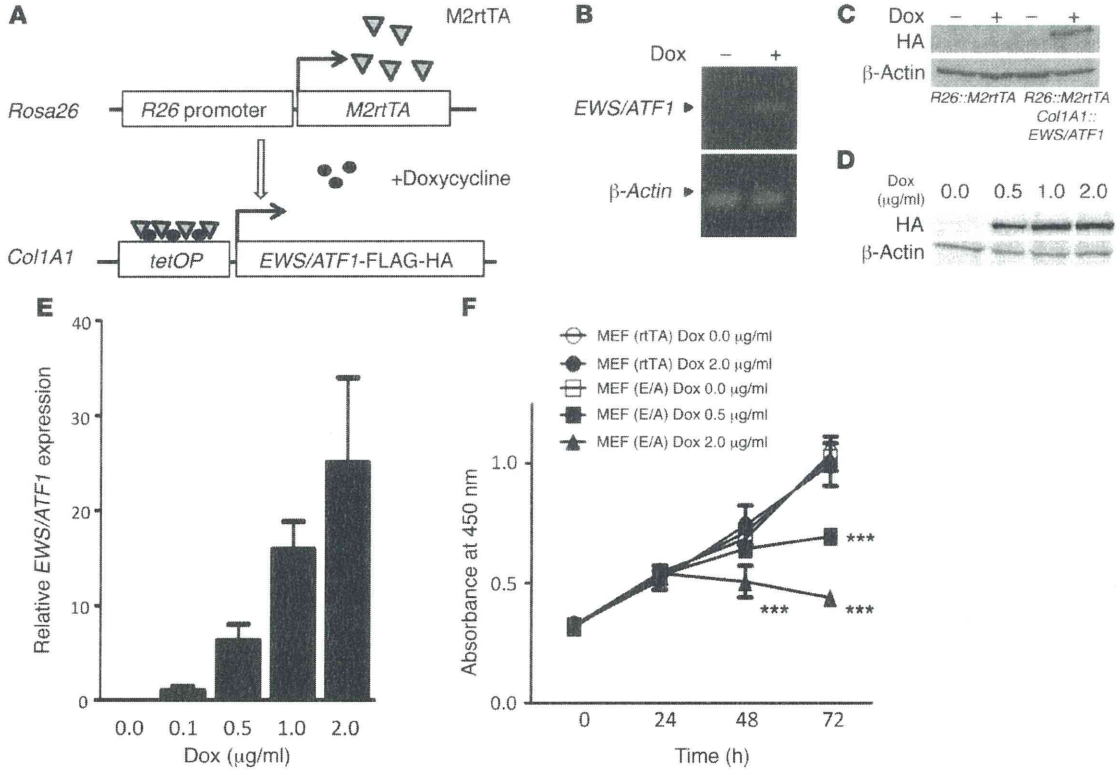

Figure 1

Inducible expression of *EWS/ATF1*. (**A**) Schematic of the doxycycline-inducible *EWS/ATF1* alleles. (**B**) *EWS/ATF1* expression in ES cells, detected by RT-PCR, after exposure to doxycycline for 12 hours. (**C**) EWS/ATF1 expression in ES cells, detected by Western blot, after exposure to doxycycline for 24 hours. (**D**) Dose-dependent induction of EWS/ATF1 protein in *EWS/ATF1*-inducible ES cells by doxycycline. ES cells were exposed to doxycycline concentrations up to 2 μg/ml for 24 hours. Western blot analysis was performed using an anti-HA antibody. (**E**) Dose-dependent doxycycline induction of *EWS/ATF1* mRNA in *EWS/ATF1*-inducible MEFs. MEFs were exposed to different concentrations of doxycycline for 24 hours. Transcript levels were normalized to β-*actin*. Data are mean ± SD ($n = 3$). (**F**) *EWS/ATF1* expression suppressed MEF growth. Cell viability was determined by WST-8 assay. Data are mean ± SD ($n = 4$). Control MEFs (rtTA) and *EWS/ATF1*-inducible MEFs (E/A) were derived from heterozygous *Rosa26::M2rtTA* and *Col1A1::tetO-EWS/ATF1* mice, respectively. ***$P < 0.001$ vs. MEF (rtTA) Dox 0.0 μg/ml, MEF (rtTA) Dox 2.0 μg/ml, and MEF (E/A) Dox 0.0 μg/ml.

a tetracycline-responsive regulatory element (Figure 1A). Upon treatment of these ES cells with doxycycline, expression of the *EWS/ATF1* fusion transcript was detected by RT-PCR (Figure 1B). We also confirmed the expression of EWS/ATF1 protein upon doxycycline treatment (Figure 1C), which was regulated in a dose-dependent manner (up to 2 μg/ml; Figure 1D).

Heterozygous *Rosa26::M2rtTA* mice with heterozygous *tetO-EWS/ATF1* allele were used to induce the *EWS/ATF1* fusion gene. Cultured murine embryonic fibroblasts (MEFs) derived from *EWS/ATF1*-inducible mice were first exposed to doxycycline to test the effect of *EWS/ATF1* expression on somatic cells. *EWS/ATF1* expression at the mRNA level was confirmed 24 hours after exposure (Figure 1E). Unexpectedly, the cell proliferation rate of MEFs decreased after *EWS/ATF1* induction in a doxycycline dose–dependent manner (Figure 1F).

EWS/ATF1 induces sarcoma formation in mice. To investigate the effect of *EWS/ATF1* expression in vivo, we treated *EWS/ATF1*-inducible mice at 6 weeks of age with doxycycline in the drinking water (50 μg/ml). The *EWS/ATF1*-inducible mice given doxycycline started to develop multiple macroscopic soft tissue tumors after 4 weeks. After doxycycline treatment, EWS/ATF1 protein was detected in a variety of tissues, including the intestine, liver, epidermis, and deep soft tissue (Supplemental Figure 1A; supplemental material available online with this article; doi:10.1172/JCI63572DS1). Doxycycline treatment for 3 months resulted in tumor formation in the deep soft tissues of all mice ($n = 39$), whereas control mice without doxycycline treatment developed no detectable tumors. *EWS/ATF1*-induced tumors typically arose in the trunks, heads, limbs, and whisker pads (Figure 2A). Macroscopically, tumors consisted of circumscribed and lobulated gray-white mass (Figure 2A). In most cases, the tumors were attached to fascia or aponeuroses (Figure 2, A and B), which indicates that the tumors specifically arose from the deep soft tissues. Importantly, 36 of 39 mice (92%) developed tumors in the trunk, which suggests that cells located in the trunk are particularly permissive for tumorigenesis by *EWS/ATF1* expression. Despite expression of EWS/ATF1 protein, no tumor formation was observed in other tissues, such as the epidermis and intestine, even in mice given doxycycline for 3 months.

Microscopic examination of these tumors revealed striking similarities to human CCSs. The tumors showed a rather uniform pattern of compact nests or fascicles of rounded or fusiform cells, which were divided by a framework of fibrocollagenous tissue (Figure 2B).